AIAA 34th Aerospace Sciences Meeting, January 1996

DYNAMIC ROLL CONTROL EXPERIMENTS USING A MOVEABLE NOSETIP

Kevin G. Peterson[§], Leigh Ann Darden[§], and Narayanan M. Komerath[¶]
School of Aerospace Engineering
Georgia Institute of Technology
Atlanta, GA 30332-0150

ABSTRACT

Rapid lateral motion of the nosetip stagnation point is used to induce yawing and rolling moments on a wing-body at angle of attack in a low-speed tunnel. The response of the lateral pressure difference across the forebody, and the rolling moment, to nosetip motion are explored. Previous work on the roll moment at zero bank angle is extended to other fixed bank angles at several sting angles. Pressure difference responds essentially at freestream convection speed to square-wave and sinusoidal nosetip excitation at frequencies of 0.1, 0.5, and 1 Hz. The pressure amplitude is insensitive to roll of 5 and -5 deg., but decreases as sting angle increases from 35° to 45°. Three angle-of-attack states are identified for forebody-wing interaction. At 45°, fast responding favorable roll-yaw coupling at finite bank angle is due to the forebody side force, with little wing interaction. At 35°, a fast adverse-roll impulse decays due to a slower favorable-roll wing vortex response. At 40°, the response is a mixture of the above two states. With the model free to roll, the moving nose controls oscillations, inducing as well as stopping wing rock oscillations rapidly. Roll-bias due to forebody asymmetry, long-time-scale vortex response, and coupling between nose motion and state-switching are observed. The state-switching and forebody-wing interactions are significantly altered when test section wall interference is reduced by a factor of 4.56 from previous experiments.

NOMENCLATURE

AR:	Aspect ratio b^2/S
b:	Wing span
C_l:	Rolling moment coefficient
C_p:	Pressure coefficient based on freestream dynamic pressure
ΔC_p:	Cp difference across forebody, Positive for suction to the right.
t:	Time
S:	Wing planform area
U_∞:	Tunnel freestream velocity
α:	Angle of attack
β:	Model yaw angle
ε:	Nose tip yaw, deg., positive to the right
Λ:	Wing leading edge sweep-back angle
ϕ:	Roll angle
σ:	Sting (roll axis) angle relative to U_∞

INTRODUCTION

This paper explores the effects of a rapidly moving nosetip on forebody lateral asymmetry and airplane rolling moment. The dynamics and control of the forebody vortex system are of interest in controlling the yawing and rolling moments on aircraft and missiles which maneuver at high angles of attack. The response of a free-flying aircraft to forebody vortex asymmetry involves nonlinear and non-monatomic and even multiple-valued dynamic phenomena of various time scales. We have developed a method to rapidly induce and modify forebody asymmetry by controlled, small-amplitude lateral displacement of the nosetip stagnation point[1]. This has enabled us to study the response of the flow and the aircraft aerodynamics to controlled dynamic asymmetry.

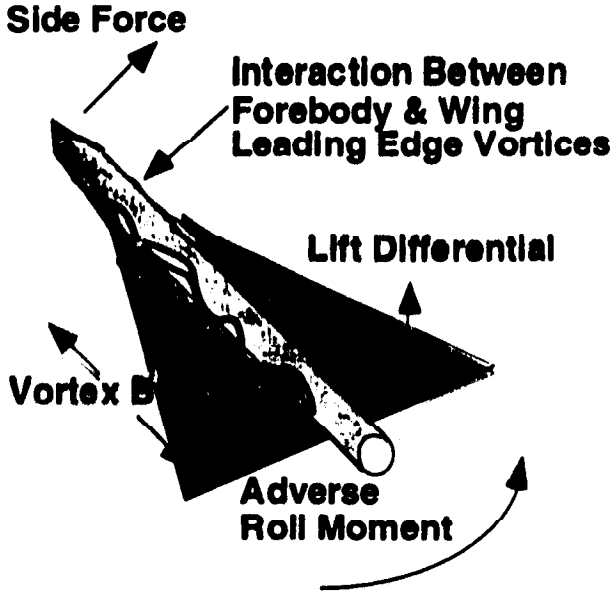

Fig. 1: Schematic of flow features and moments on a wing-body at angle of attack with moveable nosetip stagnation point.

---

§ : Graduate Student. Member, AIAA

¶: Professor. Associate Fellow, AIAA

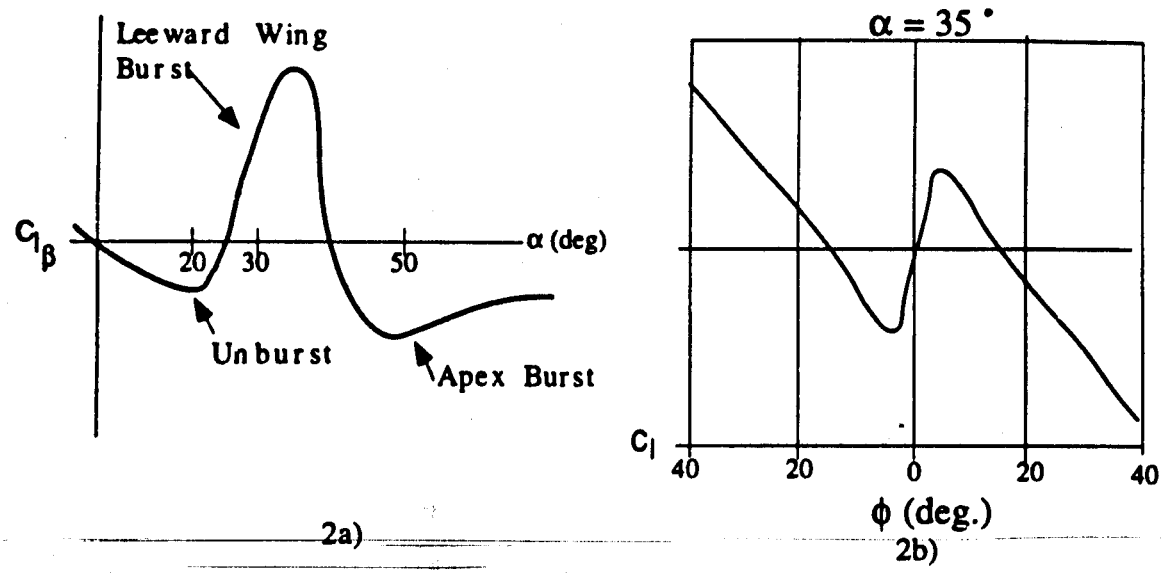

Figure 2: Qualitative features expected on a rolling wing-body at angle of attack

The nature of the problem may be seen from Figs. 1 and 2. Much of our understanding of these phenomena comes from the work of the authors of Refs. 2 - 5, and the following discussion is based in part on the recent summary given in Ref. 5. We start the discussion with a delta wing / pointed body of revolution model at a static angle of attack, with zero yaw and roll. At angles of attack above 20°, the vortices from the forebody are rarely symmetric either in strength or trajectory about the plane of lateral symmetry of the model. Their asymmetry causes a pressure difference across the forebody, and the interaction of the forebody vortices with the wing leading edge vortices causes asymmetric lift. As α increases, the wing vortices may burst over the wings. This process can be influenced by the asymmetry of the forebody vortices, with the burst location moving over the wings[6]. As the angle of attack increases beyond about 40°, the forebody vortices may pass well above the wings, and the wing vortices may be burst at their apex, so that vortex lift on the wings is not dominant. In this case, forebody asymmetry may not affect the aircraft except through the yawing and rolling moment due to the pressure difference across the forebody. From the above discussion, we see that even at a steady symmetric flight condition, there may be substantial yawing and rolling moments on a wing-body at high angles of attack.

As the model is rolled about the sting axis, the effective angles of attack and sweep change with roll angle ϕ. From Ref. 5:

$$\alpha(\phi) = \tan^{-1}(\tan\sigma \cos\phi)$$

$$\Lambda(\phi) = \Lambda_0 \pm \tan^{-1}(\tan\sigma \sin\phi)$$

Sting angle and wing aspect ratio appear to be better choices of independent variables than α and Λ. Also, the model now experiences a sideslip velocity. Fig. 2(a) shows[7,8] that the rolling moment derivative C_{l_β} is extremely sensitive, in sign as well as magnitude, to the vortex burst locations on the windward and leeward sides. The rolling moment due to sideslip is affected by the forebody asymmetry, so that the model may show a roll bias. This has been reported[9]. When the roll angle of a delta wing is changed in a quasi-steady manner, the rolling moment changes non-monatonically[5], changing from stabilizing to destabilizing and back again over a roll range of 20°, so that there are multiple trim points as shown in Fig. 2(b). Several "critical states" are seen, where the roll moment can switch between two discrete values. This switching is a phenomenon which occurs over a very long time scale. Studies on wing-body configurations[2,9] have shown that the longitudinal wing location makes a big difference. This makes the roll dynamics at high angles of attack, and their control, highly interesting. When the yaw degree of freedom is added to this problem, further interactions should be expected. The free-flying aircraft encounters these complex phenomena which have various time scales.

Our interest in the problem stems from the discovery that a small device to deflect the nosetip stagnation point can induce significant effects on the forebody vortex asymmetry, and do so quite rapidly with well-controlled temporal waveforms. The question we raised was: *What happens when a known lateral perturbation into the forebody vortex*

system is induced? The answer appeared to be that the effects on the wing rolling moment were at least as large as those induced by devices such as forebody blowing and strakes, with less mechanical complexity and a greater degree of control on both the amplitude and waveform of the perturbation. We have performed a series of experiments where the forebody asymmetry, pressure differential, and wing rolling moment could be studied independently before being coupled. In Ref. 1, we demonstrated static control of forebody vortex asymmetry using a moveable nose tip, and then showed a linear dynamic relationship (for moderate distances along the forebody) between nosetip position and vortex asymmetry at low wind speed, using a transfer function approach applied to images of the cross-flow. A long lag time was also seen in the response of the vortex flowfield; this remained unexplained until we saw the long time-scale wing response of this paper.

In Ref. 10 we measured rolling moments induced by vortex asymmetry on a rigidly constrained model, at speeds up to 23 m/s, and at zero bank and sideslip angle, for sting angles of 35°, 40°, and 45°. The tests were conducted in a 1.07 m x 1.07 m wind tunnel. The difference in surface pressure across the Zero Vorticity Contour of the forebody vortices was used as a sensor of side force asymmetry. Correlations between nose motion, wing rolling moment, and pressure difference were examined, using both square wave and sinusoidal nosetip motions at frequencies of 0.1, 0.5, and 1 Hz. Adverse yaw-roll coupling was observed at $\sigma \geq 40°$. At $\sigma \leq 35°$, the initial adverse moment effect was followed by a slower-developing, counteracting moment. This difference was attributed to the effect of vortex bursting or multiple states of wing flow separation.

The time lag in roll moment response was an order of magnitude longer than the freestream convection time, and the counteracting moment effect took another order of magnitude longer. Steady state moment variations with nose position were consistent with the adverse roll-yaw coupling at 40° and 45° sting angle, whereas the counteracting moment effects greatly reduced the moment sensitivity at $\sigma \leq 35°$. The experiments indicated the presence of at least three widely different time scales in the roll-yaw coupling of maneuvering aircraft, visible even in roll-constrained experiments. Surface pressure feedback was seen to be a viable method of measuring forebody asymmetry due to the very short time scale of its development. The results were consistent, regular and repeatable. The blockage and wall-proximity values in our experiment were conservative in comparison to those used in all except the experiments of Ref. 3, as shown in Table 1.

Table 1: Comparison of Tunnel Blockage for Various Experiments Including the Present

Expt.	%blockage @σ=45°	Wingspan/ tunnel width	Model Length/ Tunnel Height
Ref. 3	2.5	0.21	0.34
Ref. 6	8.8	0.463	0.58
Ref. 11	9.8	0.46	0.61
Ref. 9 (tunnel size 13,14)	5.8	0.40	0.60
Ref. 12	4.0	0.32	0.54
Ref. 10	4.7	0.36	0.55
Present	0.91	0.14	0.28

Present Objectives

With the zero-bank roll-constrained results in hand, and an initial demonstration of nose-tip control of roll motion, we embarked on finite-bank, roll-constrained moment measurement to be followed by controlled roll motions. We chose the John J. Harper Tunnel, with higher speeds and greater moment arms to fine-tune the precision. The test section was 4.56 times bigger for the same model and sting size; this was not expected to make any difference.

This paper reports "initial" results from the new experiments: they make sense after extensive review of previous work, and particularly after reading Ref. 5. Some of the clear and consistent results of Ref. 10 are now seen to be "beginner's luck": those results make sense only when we agree that they were seriously affected by wall interference. As seen in this paper, surface pressure differential at the forebody is not a unique indicator of wing rolling moment, because several different flow states and hence moments can exist for a given forebody differential pressure. While we are still able to induce rolling moment by moving the nose, the long-time-scale switching between states is a much more powerful phenomenon than we suspected. Under the circumstances, our objectives are modified to sort and present the phenomena encountered, give quantitative results on time scales, present the roll moments at various sting and roll angles, and demonstrate control of wing rock oscillations in free-to-roll experiments. Analysis of the data must continue for a long time.

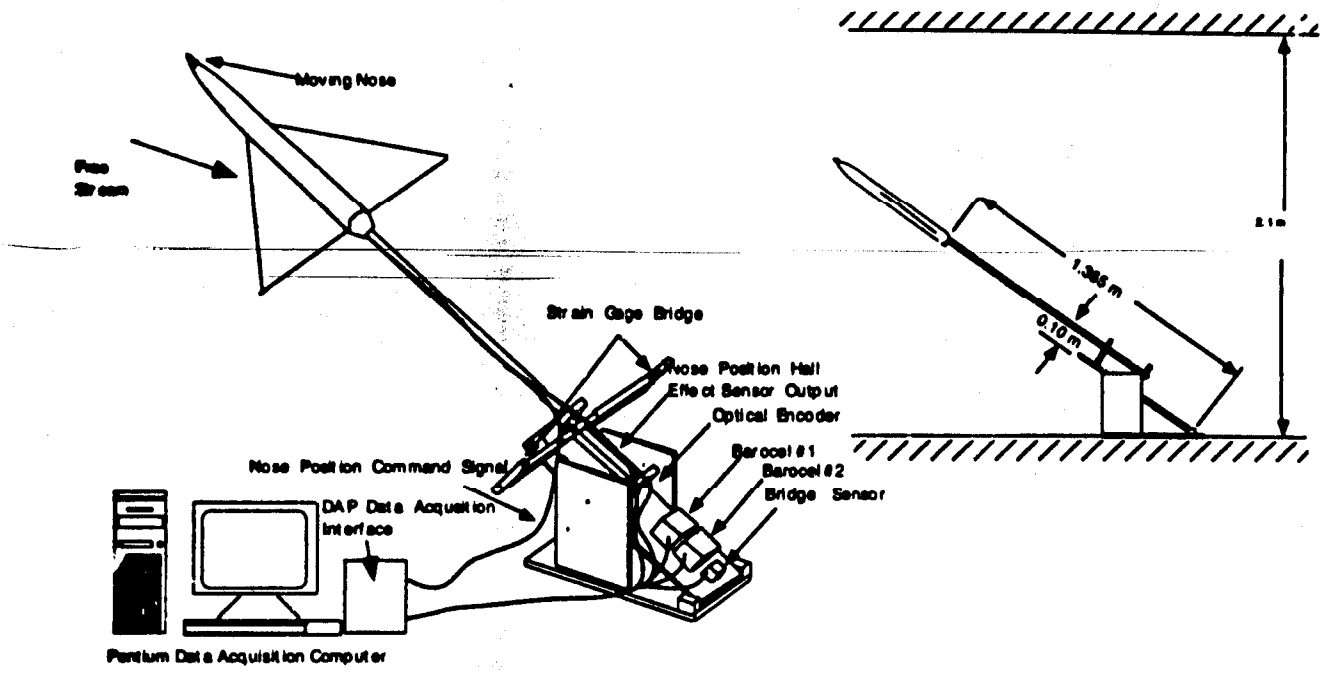

Fig. 3: AR2Δ Wing-Body Model on Roll Balance

TEST CONFIGURATION

The new experiments were performed in the 2.1 m x 2.74 m John J. Harper Wind Tunnel at the School of Aerospace Engineering. The tunnel cross-section area is 4.56 times that of the tunnel used for previous tests. The model (Fig. 3) is a delta wing/body of revolution with equal root chord and span (Aspect Ratio of 2.0) and has a cylindrical fuselage. The AR2Δ wing is a flat steel plate with sharp edges beveled at 18° on the lower surface. Its geometric sweep of 63.47° puts it between the 60° and 65° wings chosen for extensive study elsewhere. The body-of-revolution nose ends in a conical nose tip with a semi-apex angle of 15° and a length of 0.03 m. A servo motor in the fuselage rotates the nose in the yaw plane under computer control. We verified that servo actuation induces no rolling moment on the model in still air. The nose tip deflects through the yaw range $-10° < \varepsilon < 10°$. Maximum lateral deflection of the nose tip stagnation point is 8.1 mm. A 5th order polynomial was fitted to the nose-position data from a Hall effect sensor. Static pressure taps were drilled at 70° from the vertical on each side of the fuselage, with the foremost pair drilled into the wooden portion of the forebody, 140mm from the nosetip. Other taps were located 160, and 190mm aft of the nose tip. The sting is a hollow stainless steel shaft along the roll axis (Fig. 3). The instantaneous rolling moment is measured using a strain gauge balance, which is calibrated before and after the tests using known weights. The structural dynamic natural frequency in roll of this model was previously measured to be 7 Hz. No spectral peaks were visible in moment data acquired with flow off/ tunnel vibration tests.

Two kinds of experiments are presented. The first measured the forebody pressure and roll moment response to nose excitation with the balance constraining roll deflection due to aerodynamic moment to $\leq 0.25°$. At each of 11 roll settings, C_l, ε, U_∞ and ΔCp at two stations were simultaneously sampled. In the second set of experiments, the model was free to roll on bearings: ε, ϕ, U_∞ and ΔCp from two stations were sampled simultaneously. Data at 16.76, 19.81 and 22.86 m/s (55, 65 and 75 fps) are reported at each σ. Table 2 outlines test conditions. The σ settings of 35, 40, and 45° were chosen to explore forebody asymmetry control, and hence were well beyond the inburst-vortex regime, but just below the vortex shedding regime.

At each setting, square wave and sine wave variations of $\varepsilon(t)$ were used, at 0.1, 0.5, and 1Hz. Table 3 outlines data sampling parameters. Other experiments were conducted to answer questions on noise level and instrumentation response.

Table 2a: Constrained Model Test Conditions

Parameter	Test Range	Increment
Angle of Attack	35 - 45 deg.	5 deg.
Freestream Speed	55 - 75 ft/sec	10 ft/sec
Bank Angle	-5 - +5 deg.	1 deg.

Table 2b: Free-to-Roll Model Test Conditions

Parameter	Test Range	Increment
Angle of Attack	35 - 45 deg.	5 deg.
Freestream Speed	55 - 75 ft/sec	10 ft/sec

Table 3: Sampling Parameters for Square and Sine Wave Nose Deflection Tests

Wave Frequency	Sample Rate	Sample Time
1.0 Hz	50 Hz	15 seconds
0.5 Hz	50 Hz	20 seconds
0.1 Hz	50 Hz	30 seconds

Measurement Uncertainty

The strain gage balance allowed no more than 0.25 degrees roll at the highest moments measured in this paper. The uncertainty in moment measurement was 5%. The frequency response of the strain gage sensor/conditioner was flat beyond the range of interest. Static pressure difference was measured using a Barocel with a range of 10 mm Hg and a least count of one part in 10^6 of sensor range. The uncertainty in the measured values was 0.15 %.

RESULTS

The results are presented in ascending order of complexity going from the least interaction to the final cases of state-switching, wing rock control and wall interference effects. Most of the things we cannot explain are, pending flow visualization proof, attributed to the longitudinal movement of vortex burst locations, and the slow switching between states due to changes in the topology of wing flow separation, based on the explanations given in Ref. 5 and many papers by Ericsson[15]. Moving wall effects are negligible at the highest rates of nose motion presented.

1.) Effect of α on C_l Response to ε at $\phi = 0°$

a) High-α Uncoupled State:

We begin by comparing the roll response to square wave nose excitation with the model fixed at zero ϕ, where $\alpha = \sigma$. Three states are seen. The first is a very high α state shown in Fig. 4 for σ=45°. The forebody vortices appear to pass well above the wings, and wing vortex burst location appears fixed at the apex. There is a static ΔC_p due to forebody asymmetry at zero ε. Increasing ε delays vortex separation from the right side of the forebody, causing a positive ΔC_p and side force to the right. The favorable roll moment due to side force (Fig. 1) dominates Fig. 4, at excitation frequencies of 0.1 and 0.5 Hz. The moment and pressure respond in phase with the nose motion. The variations in roll moment are small.

b) Moderate α Forebody-Wing Interaction State:

The second state is shown in Figs. 5 and 6 for σ = 35°. Here forebody / wing vortex interaction dominates the roll moment response. When ε increases, the vortex strength on the right side increases, increasing suction on the right wing and causing a roll moment which is 180° out of phase with ε and ΔC_p (see Fig. 1). This initial fast impulse seen in Fig. 5 is followed by a much slower decay of C_l. This is attributed to movement of the vortex burst location.

In addition, a large spike is seen in the moment data of Fig. 5 from 0 - 5 seconds and again from 20 - 25 seconds. Figure 6, illustrates that this is a repeatable event. Thus, these moment spikes are part of a larger periodic event, which can only be described as "quasi-repeatable": it happens in every run with "more or less" the same time scale. They appear to be part of a significant phenomenon with a very long time scale.

c) Intermittent Interaction State:

In studying Fig. 7 for σ = 40° one should note that there is some steady asymmetry in the vortex system. Thus the response to positive and negative ε need not be symmetric. Allowing for this, Fig. 6 shows that each excitation of the nose creates an initial transient peak in phase with the previously existing pressure distribution. This corresponds to the 45° state. The transient behavior is followed by a return to a steady state 180° out of phase with ε. This corresponds to the lower alpha state.

2.) Rolling Moment Variation for $-5° \le \phi \le 5°$.

Figure 8 summarizes how the roll moment induced by a 10-degree ε deflection varies with ϕ in the range $-5° < \phi < 5°$ for the 3 σ states. At σ = 45°, ΔC_l remains small. At σ = 35°, roll moment coefficients as high as 0.075 are induced by stagnation point movement. The highest response within this roll range occurs at zero roll. We also see that the ΔC_l for positive roll angles is about twice the corresponding values for negative roll angles.

3.) Pressure Response Variation for $-5° \le \phi \le 5°$.

It was found that the pressure response on the forebody was independent of the frequency of square wave nose excitation. Fig. 9 presents

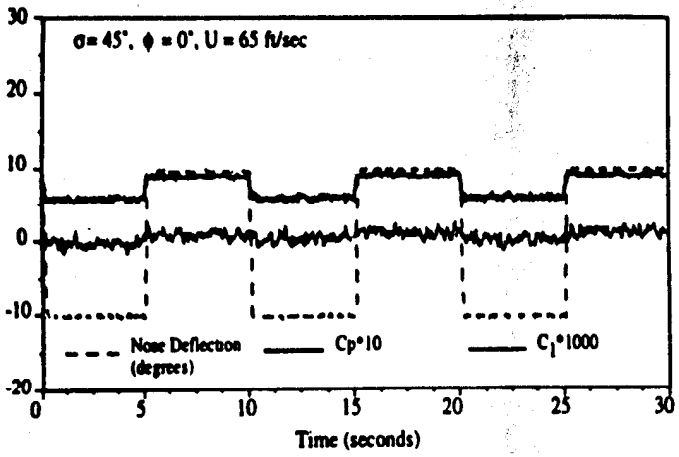

Figure 4: Time History of ΔC_p and C_l Induced by Nose Excitation of 0.1 Hz at σ=45°

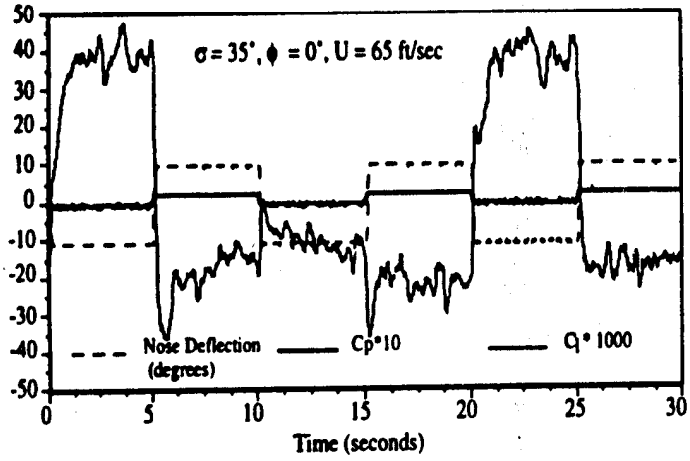

Figure 5: Time History of ΔC_p and C_l Induced by Nose Excitation of 0.1 Hz at σ=35°

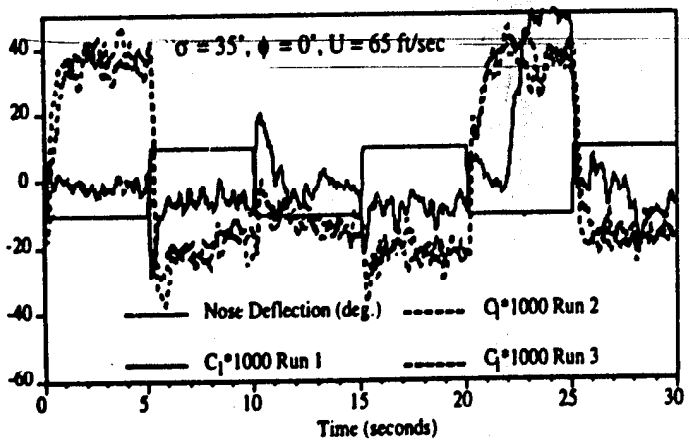

Figure 6: Three Data Sets of C_l Induced by Nose Excitation of 0.1 Hz at σ=35°

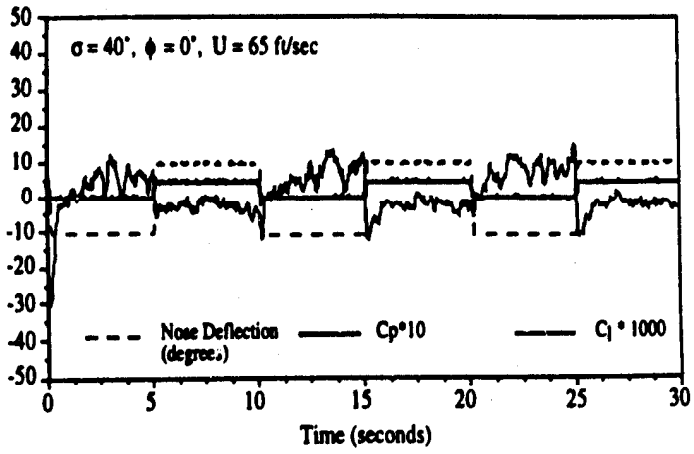

Figure 7: Time History of ΔC_p and C_l Induced by Nose Excitation of 0.1 Hz at σ=40°

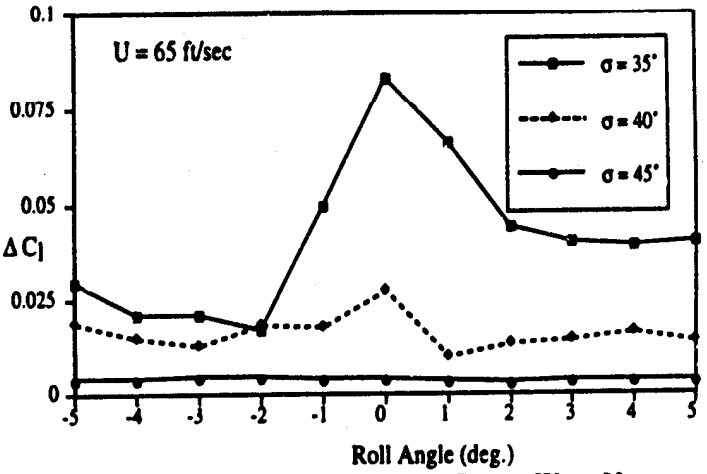

Figure 8: Average ΔC_l Induced by Square Wave Nose Excitation of 0.1 Hz

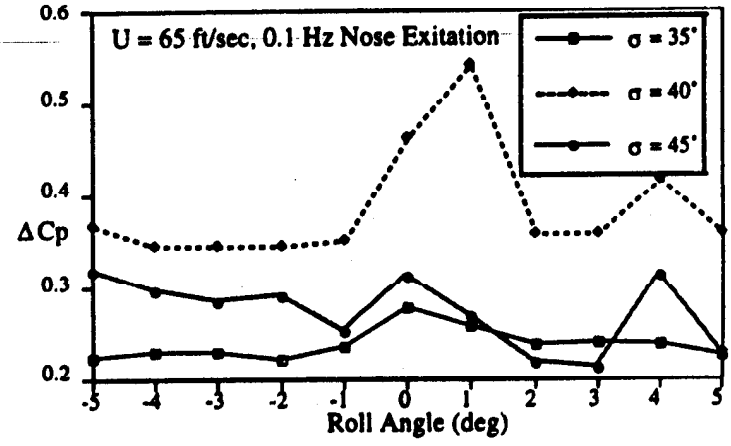

Figure 9: Average ΔC_p Induced by Square Wave Nose Excitation of 0.1 Hz

pressure response data for square wave nose motion over the roll range $-5^\circ < \phi < 5^\circ$ for the 3 σ values. This explains the results of Fig. 8 partially.

4.) Roll Moment Response Indicates Different Behavior for Positive and Negative Bank Angles

Comparing the C_l and ΔC_p responses to ε at similar test conditions revealed that the system behavior differs between right and left bank angles. Figs. 10 and 11 compare the time domain response to nose excitation of 0.1 Hz for $\phi = \pm 4^\circ$. The magnitude of the ΔC_p at the forebody remains about the same for the two bank conditions. However, the roll moment coefficient magnitude is greater for the right bank angle than for the left. In addition, the data contains less noise for the right bank attitude than for the left. At $\phi = +4^\circ$, (Fig. 11) we no longer see the characteristic peak in moment response followed by a return to some steady state condition for each nose motion. In fact, when the nose is moved to the left an undershoot followed by a rise to a steady state condition is seen. Since the pressure response is similar between the two cases, it appears that the asymmetry in roll moment occurs somewhere in the wing leading edge vortex interaction region.

5.) Time Lags in the Moment Response

We now proceed to examine the various time scales in the problem. The ΔC_p response is seen to occur essentially within the convection time at the first two sets of pressure taps. The pressure response at the taps near the wings were much harder to interpret. The moment response, however, involved substantial lags.

Fig. 12 presents the average time lag in C_l response to a square wave $\varepsilon(t)$ of 0.5 Hz at $\sigma = 35^\circ$. The behavior is similar at each of the three U_∞ settings. The shortest lag is about 0.1 seconds at $\phi = -1^\circ$; at 25 m/s, the convection time from the nosetip to the wing trailing edge is only 0.02 seconds. The longest lag is 0.3 seconds at $\phi = -3^\circ$.

Fig. 13 which presents the average roll moment time lag for each angle of attack, indicates that the roll moment responds quicker at 45° than at the other two angles of attack. Fig. 12 illustrates that freestream speed is a secondary issue in determining this time lag.

6.) Long Time Scale Phenomena

Two kinds of phenomena are shown. One is a quasi-repeatable large-amplitude moment response which occurs about once every three cycles of square-wave nose excitation as seen in Fig. 5 and 6. The repetition time scale is on the order of 20 seconds, but the moment responds quickly to nose motion.

The second is the "switching" phenomenon shown in Fig. 14 This has been reported before in Ref. 11 in steady-state tests. Here we see it occurring despite the presence of the square-wave or sine-wave perturbation caused by the nose motion. The perturbation is simply superposed on a mean value which changes by a large amount with an apparent period of about 40 seconds! This was seen numerous times, and is not explicable by instrumentation error, tunnel speed changes or any such explanation which we could test. In most cases, the moment went from negative to positive; one case was however seen where it switched abruptly from positive to negative.

7.) Free-to-Roll Tests

The above data paint a rather bleak picture for the possibility of controlling roll oscillations of a free-flying aircraft using any forebody control device. However, free-to-roll tests showed otherwise. Several free-to-roll tests were performed, which are shown on a videotape accompanying this paper. By moving the nosetip through 10 degrees or less, the model was forced to oscillate in roll of up to 20 degrees amplitude, as shown in Fig. 15. Static deflection of the nose caused minimal changes in the roll attractors while nose oscillation was able to force roll attractor switching to some extend at all angles of attack. The wing-rock phenomenon was also encountered. Fig. 16 presents bank angle and pressure differential response data to nose excitation of 0.2 Hz at $\sigma = 40^\circ$. We see that for $\varepsilon > 0$, wing rock at a frequency of 1.6 Hz is established. Further, when the nose returns to a left deflection, the wing rock phenomenon is neutralized immediately.

8) Wall interference

The data at $\sigma = 35^\circ$, 40°, and 45° were an unpleasant surprise because it appeared that we had moved into a higher α regime than intended. The level of unsteadiness and especially the long-time-scale switching were quite unexpected, based on our experience with the results of Ref. 10 obtained in the 1.07m x 1.07m tunnel with the same model and similar sting set-up. This led to much trouble-shooting, but eventually we realized that the data of Ref. 10 corresponded to sting angles about 2 to 5 degrees lower than those used in the present experiments. A consideration of the angle of attack induced by the proximity of the upper wall appears to resolve the difference. Table 1 might explain why some of these problems have not plagued more researchers in the past.

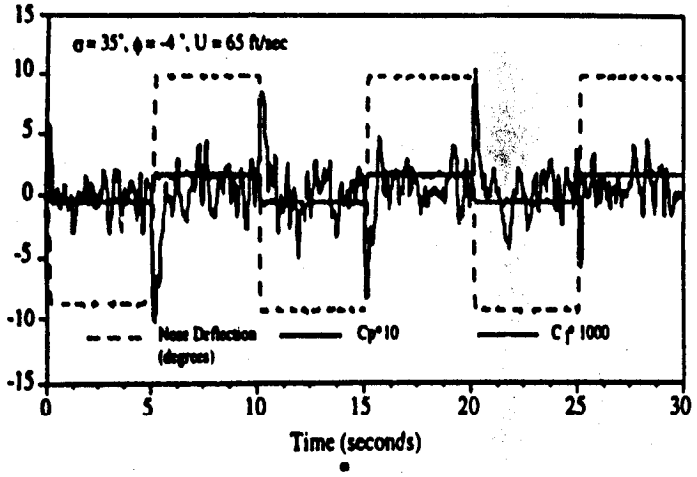

Figure 10: Time History of ΔC_p and C_l Induced by Nose Excitation of 0.1 Hz at σ=35°, ϕ= -4°

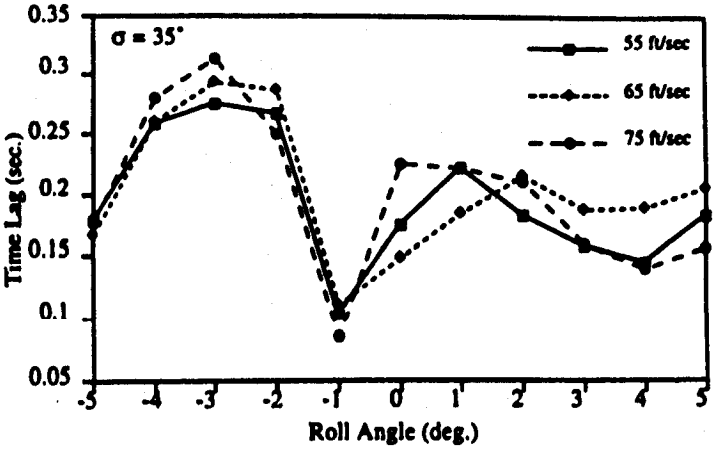

Figure 12: Rolling Moment Time Lag Variation with Roll Angle, 0.1 Hz Nose Excitation

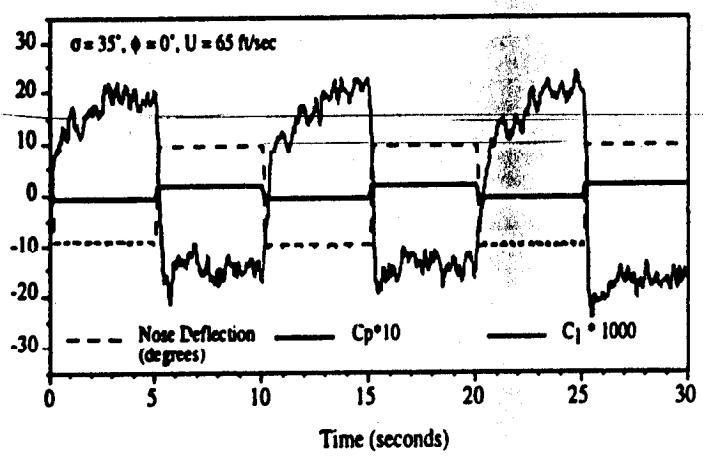

Figure 11: Time History of ΔC_p and C_l Induced by Nose Excitation of 0.1 Hz at σ=35°, ϕ= +4°

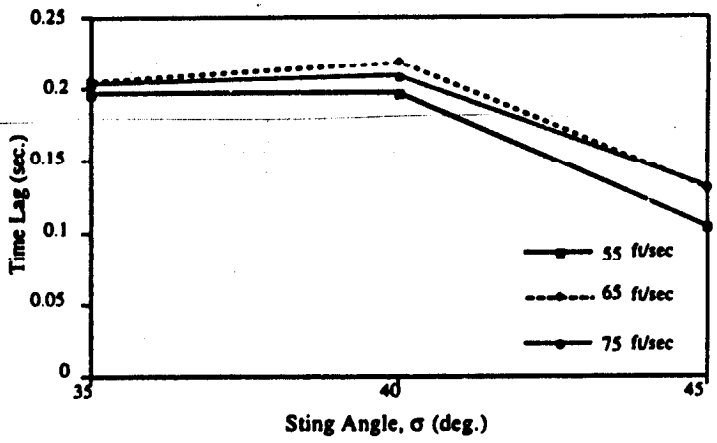

Figure 13: Rolling Moment Time Lag Variation with Sting Angle, 0.1 Hz Nose Exitiation

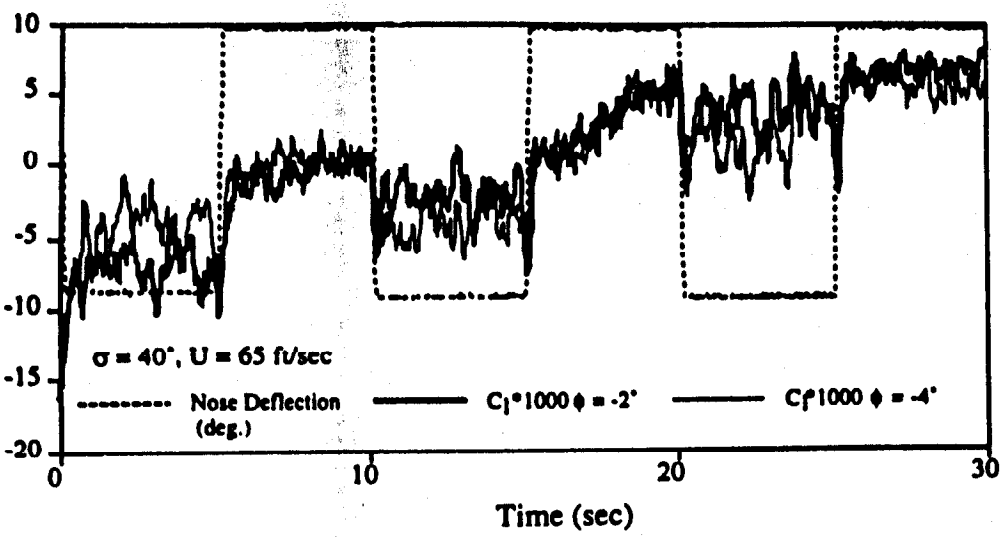

Figure 14: Moment Switching Phenomenon

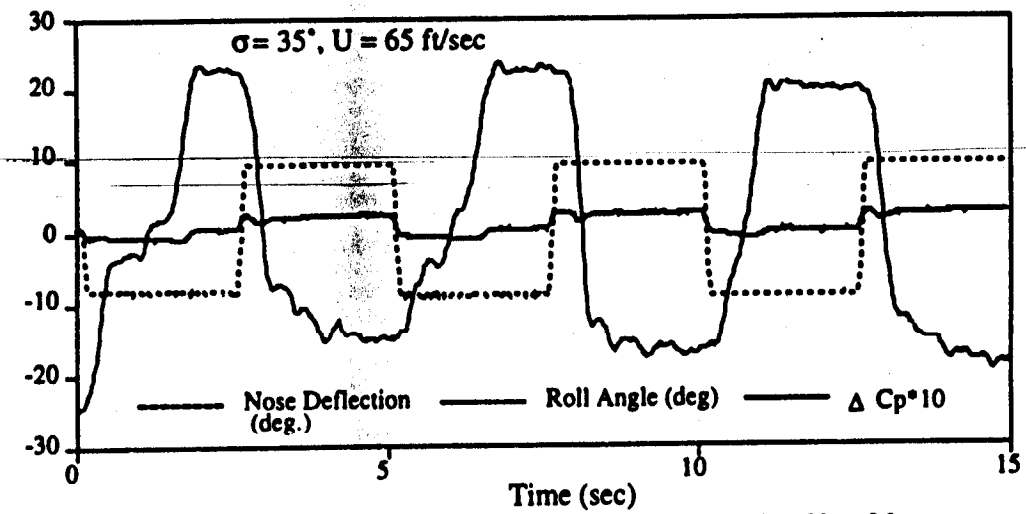

Figure 15: Free-to-Roll Roll Attractor Switching Induced by Nose Movement

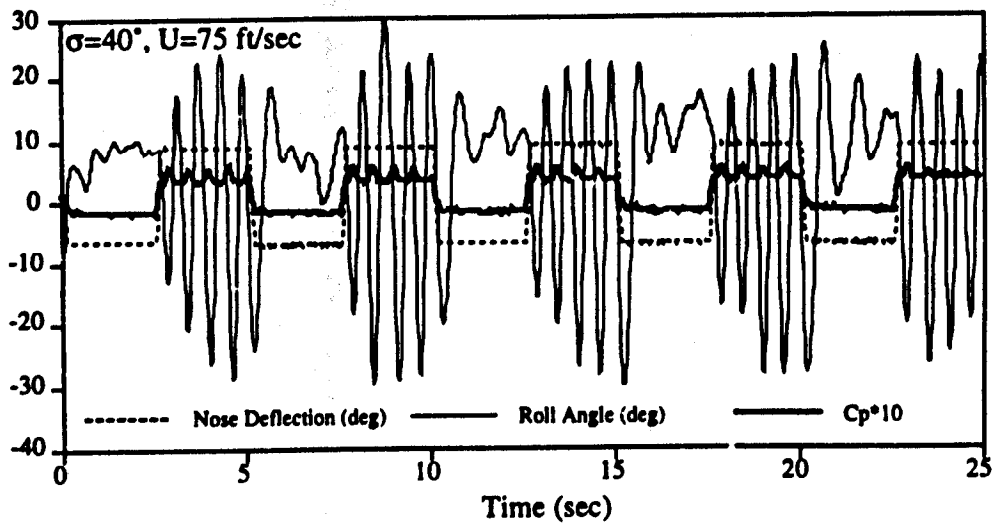

Figure 16: Initiation and Elimination of Wing Rock via Nose Deflection

9) Time Scales

We now see the presence of several time scales in the response of the wing-body flow to nose excitation. T1, the time for the forebody pressure to respond to nose motion, is very short, being essentially the convection time. T2, the time for the roll moment due to sideslip, is also short, being limited primarily by the model inertia. T3, the time for the wing vortex system to respond to nose excitation is about 10 to 30 times the convection time. T4, a time scale for some resonant response to nose excitation, is roughly 10 to 20 seconds, whereas the convection time is in milliseconds. T5 is an even longer time scale for the baseline roll moment to switch from positive to negative and vice versa. This is of the order of 40 seconds.

CONCLUSIONS

We have used a moving nosetip stagnation point to perturb the vortex system over a wing/body at angle of attack. Rolling moments and lateral pressure differences have been related to nose movement in tests at small fixed roll angles, and the nose position, roll angle, and pressure difference have been measured in free-to-roll tests with imposed nose motion.

Specific conclusions:

1. At zero roll, three angle of attack states are identified. At α=45° the moment response is due to forebody side force, and is in phase with the nose motion. The moment amplitude is extremely small, and the time lag in moment development is also small.

2. The second state is at α = 35°, where the moment response is dominated by the response of the wing vortices to interaction with the forebody vortices. The response starts with a quick adverse-yaw impulse, followed by a slower return to steady-state. Moment coefficient amplitudes due to nose movement reach 0.075.

3. The third state is a mixture of the above two, and is seen at α = 40°.

4. The time scale of response is sensitive to roll angle and much less sensitive to freestream speed. The average response time at σ = 35° ranges from 10 to 30 times the convection time.

5. Forebody pressure difference reacts essentially at convection speed to nose movements.

6. A quasi-repeatable large-amplitude response to nose motion is observed, with time scales of roughly 20 seconds at σ = 35°

7. A switching with very long time scale (estimated at 40 seconds) is observed in many runs, with the nose-induced moment excitation superposed on a quasi-steady state which changes by a large amplitude.

8. In free-to-roll tests, controlled roll oscillations with up to 20 degrees amplitude are induced on a high-inertia model by moving the nose.

9. Wing rock oscillations are both induced and eliminated by moving the nose.

10. Results obtained with tunnel blockage of 5% are seen to require corrections of up to 5° of incidence to match results obtained with blockage of 1.2%. Long time-scale phenomena seen in the latest tests were not seen in tests conducted on the same model in a tunnel where blockage was 5%.

11. Two different long time scales must be added to those previously observed.

ACKNOWLEDGMENTS

This work was performed under AFOSR AASERT Grant F49620-93-1-0342, monitored by Maj. Daniel Fant and Dr. Len Sakell. The first author receives support from a Mercury Seven Foundation Fellowship, and the second from an NSF Graduate Fellowship. Assistance from members of the Experimental Aerodynamics Research Team is gratefully acknowledged.

REFERENCES

1. Darden, L.A., Komerath, N.M., "Forebody Vortex Control At High Incidence Using A Moveable Nose Stagnation Point", AIAA 95-1775, June 1995.

2. Brandon, J.M., Nguyen, L. T., "Experimental Study of Effects of Forebody Geometry on High Angle-of-Attack Stability," *Journal of Aircraft*, Vol. 25, No. 7, July 1988, p. 591-597.

3. Huang, X.Z., Hanff, E.S., Jenkins, J.E., Addington, G., "Leading-Edge Vortex Behavior on a 65-degree Delta Wing Oscillating in Roll," AIAA 94-3507, August 1994.

4. Ericsson, L.E. Reding, J.P., "Asymmetric Vortex Shedding from Bodies of Revolution," *Tactical Missile Aerodynamics*, Vol. 104, 243-296.

5. Jenkins, J.E. and Hanff, E.S., "Highlights of the IAR/WL Delta Wing Program, "Proceedings of Workshop III: Delta Wings, Unsteady Aerodynamics and Modeling," Baltimore, Aug. 95.

6. Hall, R., "Influence of Forebody Cross-Sectional Shape on Wing Vortex-Burst Location," *Journal of Aircraft*, Vol. 24, No. 9, 1987, pp. 645-652.
7. Skow, A.M., "Control of Advanced Fighter Aircraft," AGARD FDP-VKI Lecture Series, 1983. Qualitative plot reproduced in Rom, J., *"High Angle of Attack Aerodynamics"*, Springer-Verlag, New York, 1992, p. 49.
8. Rom, J., *"High Angle of Attack Aerodynamics,"*. Springer-Verlag, New York, 1992
9. Williams II, D., Nelson, R., Ericsson, L., "Influence of Wing-Forebody Separation on Forebody-Induced/Driven Wing Rock," AIAA 95-3441, August 1995.
10. Darden, L.A., Peterson, K. G., Komerath, N.M., "Vortex Control Using a Moving Nose with Pressure Feedback", AIAA Paper 95-3468, August 1995.
11. Pamadi, B.N., Rao, D.M., Niranjana, T., "Wing Rock and Roll Attractor of Delta Wings At High Angles of Attack", AIAA 94-0807, Jan 1994.
12. Celik, Z.Z., Pedreiro, N., and Roberts, L., "Dynamic Roll and Yaw Control by Tangential Forebody Blowing", AIAA 94-1853, June 1994.
13. Arena, A.S., Jr., Nelson, R.C., "Experimental Investigations on Limit Cycle Wing Rock of Slender Wings", *Journal of Aircraft*, Vol. 31, No. 5, Sept.-Oct. 1994, pp. 1148-1155.
14. Grismer, D.S. and Nelson, R.C., "Double-Delta-Wing Aerodynamics for Pitching Motions With and Without Sideslip," *Journal of Aircraft*, Vol. 32, No. 6, Nov.-Dec. 1995, p. 1303-1311.
15. Ericsson, L., "Wing Rock Analysis of Slender Delta Wings, Review and Extension," *Journal of Aircraft*, Vol. 32, No. 6, Jul. - Aug. 1995, pp. 1221-1226.